Local modes of bond-centered hydrogen in Si:Ge and Ge:Si

R. N. Pereira* and B. Bech Nielsen
Institute of Physics and Astronomy, University of Aarhus, DK-8000 Aarhus, Denmark

L. Dobaczewski
Institute of Physics, Polish Academy of Sciences, Warsaw, Poland

A. R. Peaker
Centre of Electronic Materials, UMIST, Sackville Street, P.O. Box 88, Manchester, M60 1QD United Kingdom

N. V. Abrosimov
Institute of Crystal Growth, D-12489 Berlin, Germany

(Received 20 December 2004; revised manuscript received 24 February 2005; published 4 May 2005)

Local vibrational modes of bond-centered hydrogen have been identified in Ge-doped Si (Si:Ge) and Si-doped Ge (Ge:Si) with *in-situ*-type infrared absorption spectroscopy. The infrared absorbance spectra recorded at 8 K immediately after implantation of the very dilute Si:Ge and Ge:Si alloys with protons reveal in each case four lines located at ~2000 and ~1800 cm^{-1}, respectively. The dominating band in all spectra arises from quasi-isolated positively charged bond-centered hydrogen (H_{BC}^{+}) centers, whereas the remaining features originate from different H_{BC}^{+} defects perturbed locally by a nearby Ge in Si:Ge or Si in Ge:Si located in the first-, second- and third-nearest neighbor sites. These assignments are based on the analysis of the local mode frequencies and their absorption intensities, together with the isotopic shifts observed when hydrogen is replaced by deuterium, and the thermal stability of the modes. Our results are compared with previous experimental and *ab-initio* theory investigations.

DOI: 10.1103/PhysRevB.71.195201 PACS number(s): 61.72.Tt, 61.72.Ji, 63.20.Pw, 61.72.Cc

I. INTRODUCTION

Hydrogen is an important impurity atom in semiconductor technology because it is present in most of the processing steps of these materials. Due to its high diffusion rate and reactivity hydrogen is present in a number of defects, such as dopant-hydrogen pairs which lead to the neutralization of donors and acceptors. The most fundamental hydrogen defects in group IV semiconductors are interstitial hydrogen atoms occupying the bond center site (H_{BC}) or the interstitial tetrahedral site. The structure of H_{BC} is sketched in Fig. 1(a). This defect has been investigated both in silicon and germanium by a number of techniques, like Fourier-transform infrared absorption spectroscopy (FTIR),[1–5] deep-level transient spectroscopy,[6–8] electron paramagnetic resonance,[9,10] channeling,[11] muonium spin resonance,[12] and *ab-initio* theory.[13–17] Light impurity atoms such as hydrogen induce local vibrational modes (LVMs) with frequencies that are well above those of the crystal phonons, which facilitates the detection of these defects by FTIR. In fact, most of our knowledge about the properties of hydrogen in both silicon and germanium has been obtained by investigations of hydrogen-related LVMs.

In the positive and neutral charge states hydrogen occupies the position midway between two bonded Si atoms, resulting in a defect with D_{3d} symmetry.[13–18] A simple molecular-bonding analysis shows that the 1*s* orbital of hydrogen couples to the bonding state, which results from the symmetric combination of the two sp^3 hybrids residing on the silicon neighbors, to form a three center bond $sp^3(\mathrm{Si}) + s(\mathrm{H}) + sp^3(\mathrm{Si})$.[19] For positively charged hydrogen the three center orbital is fully occupied, whereas for the neutral charge state the additional electron enters the antibonding state $sp^3(\mathrm{Si}) - sp^3(\mathrm{Si})$ with a node at the hydrogen atom. Previous FTIR measurements revealed that positively charged bond-centered hydrogen induces an infrared-active LVM with frequency at 1998 cm^{-1} in Si and at 1794 cm^{-1} in Ge.[2,4] This mode is an A_{2u} asymmetic stretching mode where the

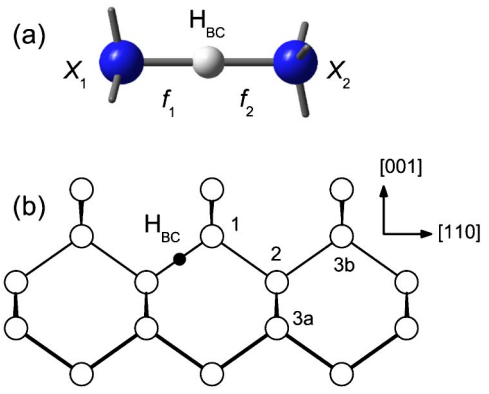

FIG. 1. (a) Basic structure of interstitial hydrogen in the bond center site, where X_i (with $i=1,2$) represent Si and/or Ge atoms. f_1 and f_2 denote the harmonic force constants of the X_1-H and X_2-H bonds, respectively. (b) The $(\mathrm{Ge_sH_{BC}^{+}})_j$ and $(\mathrm{Si_sH_{BC}^{+}})_j$ configurations correspond to complexes where substitutional Ge (Ge_s) and substitutional Si (Si_s), respectively, are placed in the site $j=1$, 2, 3a, 3b with respect to the H_{BC}^{+}. The configurations $(\mathrm{Ge_sH_{BC}^{+}})_\infty$ and $(\mathrm{Si_sH_{BC}^{+}})_\infty$ correspond to complexes where, respectively, Ge_s and Si_s are located relative to H_{BC}^{+} farther away than site 3b.

oscillations are mainly localized on the hydrogen atom. In silicon, H_{BC}^{+} is stable at temperatures up to ~150 K, whereas in Ge it is thermally stable up to ~210 K. Although these centers are unstable at room temperature, they can be detected by *in-situ*-type measurements after low temperature proton implantation.

At present, much attention is focused on silicon-germanium (SiGe) alloys due to their beneficial properties that may lead to improved devices.[20,21] Among these properties are high carrier mobilities[22] that are important for ultrafast electronic devices,[23,24] and the use of strained SiGe materials in band-edge engineering for optoelectronic devices.[25–27] Despite the presence of hydrogen, for example in the CVD growth of SiGe,[28,29] its properties in SiGe have not been amply investigated. In particular, little is known about the structure and stability of bond-centered hydrogen species in this material, apart from the deep-level transient spectroscopy (DLTS) investigations mentioned below. SiGe alloys form a fully miscible solid solution with a face-centered cubic lattice structure. In dilute SiGe crystals the least abundant element (the minority species) produces a randomly distributed internal strain, which is absent in pure silicon and pure germanium. In Si-rich SiGe, the substitutional Ge atoms form four Si—Ge bonds that are longer than the averaged Si—Si bond.[30] This induces strain locally that causes compression of some Si—Si bonds while others are elongated in the vicinity of the Ge atoms. In Ge-rich SiGe, the situation will be very similar since perturbed Ge—Ge bonds will exist in the vicinity of the silicon atoms.

The formation of the H_{BC} defect involves two opposing energy terms: (a) the lowering of the energy that results from the formation of the three atom bond X_1-H-X_2 and (b) the increase in energy associated with the outwards displacement of the two host atoms bonded to hydrogen. The energy term (b) will depend on the length of the Si—Si (or Ge—Ge) bond before the hydrogen atom moves in and, henceforth, it is more energetically favorable to add an hydrogen to an elongated bond than to a compressed one. This implies that the X_i-H bond lengths of H_{BC}^{+} will depend on the stress conditions of the pertinent bond-center site, e.g., compressed Si—Si (or Ge—Ge) bonds result in shorter X_i-H bonds. As a result of the different bond lengths the vibrational frequencies associated with the stretching of the X_i-H bonds will differ from site to site, as well as the thermal stability of different H_{BC}^{+} sites. Shorted X_i-H bonds result in H_{BC}^{+} centers vibrating at higher frequencies and with lower thermal stability. This means that the frequencies (and thermal stabilities) of different H_{BC}^{+} sites will correlate with the local strain conditions of the bond center site that accommodates the hydrogen atom. In this context, the H_{BC}^{+} centers in dilute SiGe alloys are especially interesting since the local strain imposed by the minority species may be probed by measuring the strain-induced LVM frequency shifts on H_{BC}^{+} sites neighbored by the minority species, with respect to the frequencies observed for *isolated* H_{BC}^{+} centers. Knowing the local strain properties of SiGe is essential to clarify the origins of the unique properties of this material and to develop the device potential of these materials. Another interesting point is related to the fact that in silicon more stable configurations of H_{BC} centers are formed in the vicinity of substitutional carbon[31,32] and interstitial oxygen impurities.[7,33,34] In this context, the investigation of whether H_{BC} in silicon (or germanium) is also thermally stabilized by the presence of Ge (or Si) is of current technological interest.

The influence of germanium in the vicinity of bond-centered hydrogen has been examined recently in an *in-situ* Laplace deep-level transient spectroscopy (DLTS) study of proton-implanted Si-rich SiGe alloys.[35] A comparison of the Laplace-DLTS spectra of the proton-implanted alloys with a reference spectrum of pure Si led to the identification of two levels related to bond-centered hydrogen defects. One of these is essentially the same as the $H_{BC}(0/+)$ donor level in silicon, denoted $E3'$,[6,36] whereas the other, labeled $E3'$(Ge), is somewhat shallower and has been ascribed to a H_{BC} defect locally perturbed by a substitutional Ge placed as a nearest neighbor to one of the two silicon atoms attached to the hydrogen. Below, this structure shall be denoted by $(Ge_sH_{BC})_2$ as shown in Fig. 1(b). Annealing data shows that the $E3'$(Ge) structure is slightly less thermally stable than the $E3'$ structure, probably due to the compressive strain produced by the neighboring Ge. The formation of such compressed configuration of bond-centered hydrogen in dilute SiGe alloys is supported by LVM infrared absorption data.[37] Two FTIR lines at around 2000 cm^{-1} and split by ~7 cm^{-1} were detected after low temperature proton implantation into Si-rich SiGe crystals, and were assigned to H_{BC}^{+} species. The lower frequency line was ascribed to locally unperturbed H_{BC}^{+} centers, whereas the higher frequency line was assigned to H_{BC}^{+} lying in a Si—Si bond compressed by a neighboring Ge atom. The latter defect is likely to be identical to the one responsible for the $E3'$(Ge) DLTS transition.

Recently, the total energies and the LVM frequencies of hydrogen in different sites around Ge in Si-rich SiGe and around Si in Ge-rich SiGe were calculated by an *ab-initio* supercell method.[17] The different configurations of the H_{BC} defect considered in the calculations are sketched in Fig. 1(b). It was found that the frequency of H_{BC}^{+} correlates with the available space for H in the bond center site. In Si-rich SiGe, Ge tends to compress the neighboring Si—Si bonds, contrarily to Si in Ge-rich SiGe that produces a tensile strain on the neighboring Ge—Ge bonds. Hence, for H_{BC}^{+} sites in Si-rich SiGe the highest frequency is obtained when Ge is located in the second-nearest neighbor position and drops as the Ge is moved farther away from the H. The findings in Ge-rich SiGe are a mirror image of those obtained in Si-rich material. In Ge-rich SiGe, the lowest mode frequency is obtained with the Si at the next-nearest lattice site and the frequency increases as the Si is placed farther away. In addition, the authors suggest that the Si—H_{BC}^{+}—Ge configuration gives rise to the lowest frequency for H_{BC}^{+} in Si-rich SiGe, whereas in Ge-rich SiGe its frequency is the highest among all H_{BC}^{+} defects. The different H_{BC}^{+} configurations were found to be energetically degenerate within the accuracy of the calculations, in agreement with an earlier density-functional study of H_{BC}^{+} in Si-rich SiGe.[38]

The few reported experimental investigations on H_{BC}^{+} in SiGe mentioned above[35,37] corroborate the theoretical results. However, the great majority of the H_{BC} structures considered theoretically have remained unobserved so far. Hence, no

experimental evidence for the formation of the Si—H_{BC}^{+}—Ge complexes in SiGe have been reported and the properties of hydrogen in Ge-rich SiGe have not yet been investigated.

Our purpose in this article is to report on a comprehensive study of interstitial hydrogen in both Si-rich and Ge-rich SiGe. Ge-doped silicon and Si-doped Ge crystals are implanted at low temperatures with protons or deuterons and studied by *in-situ*-type FTIR. LVMs arising from different configurations of H_{BC}^{+} are identified and compared with those previously observed in pure Si and pure Ge. We examine the hydrogen isotope shifts and demonstrate the formation of Si—H_{BC}^{+}—Ge centers in both Si-rich and Ge-rich SiGe material. In addition, we identify the local modes of Si—H_{BC}^{+}—Si (or Ge—H_{BC}^{+}—Ge) in the vicinity of a single Ge (or Si) atom placed in the second- and third-nearest neighbor sites in dilute SiGe alloys. The thermal stability of all the bond-centered hydrogen species is investigated through the study of the annealing response of the mode intensities.

II. EXPERIMENTAL DETAILS

The experiments presented in this paper were performed on Ge-doped Si and Si-doped Ge samples chosen so that the concentration of the dopant is about the same in the two crystals. The Ge concentration is 0.9 ± 0.1 at.% in the case of the Si crystal and the silicon concentration is 1.2 ± 0.1 at.% for the Ge sample, as measured by Rutherford backscattering spectrometry (RBS). The Ge-doped Si sample we label Si:Ge and similarly the Si-doped Ge sample we denote Ge:Si. The samples are unstrained float-zone (Si:Ge) and Czochralski-grown (Ge:Si) bulk crystals with phosphorous concentrations of about 5×10^{15} cm^{-3}. The concentrations of oxygen and carbon in the crystals are less than 1×10^{16} cm^{-3}. The crystals were implanted with protons (or deuterons) using different energies in the range 1.0–2.5 MeV and the dose at each energy was adjusted to yield fairly uniform H (or D) concentration profiles over a range of ~50 μm (or ~35 μm) in the case of the Si:Ge sample, and over a range of about 35 μm (or ~25 μm) for the Ge:Si crystal. The total implantation doses were determined to obtain a concentration of the implanted species of $4-5\times10^{18}$ cm^{-3}. To guarantee a uniform lateral distribution of the implanted species, the ion beam was swept both vertically and horizontally. At each energy, the beam current was measured before the implantation in order to estimate the time needed to reach the desired dose. The samples were mounted in a helium cryostat attached to the accelerator beamline and the samples' temperature during the implantations was kept below 15 K. After the implantation, the cryostat was detached from the beamline and moved to the infrared absorption spectrometer. During the transportation the sample temperature never increased above 20 K, which prevented the diffusion of the implanted H or D. The infrared absorption spectra were recorded with a Nicolet, System 800, FTIR spectrometer equipped with a Ge—KBr beamsplitter, a glowbar light source, and a mercury-cadmium-telluride detector. All spectra were recorded at ~8 K with an apodized resolution of 0.5 cm^{-1}.

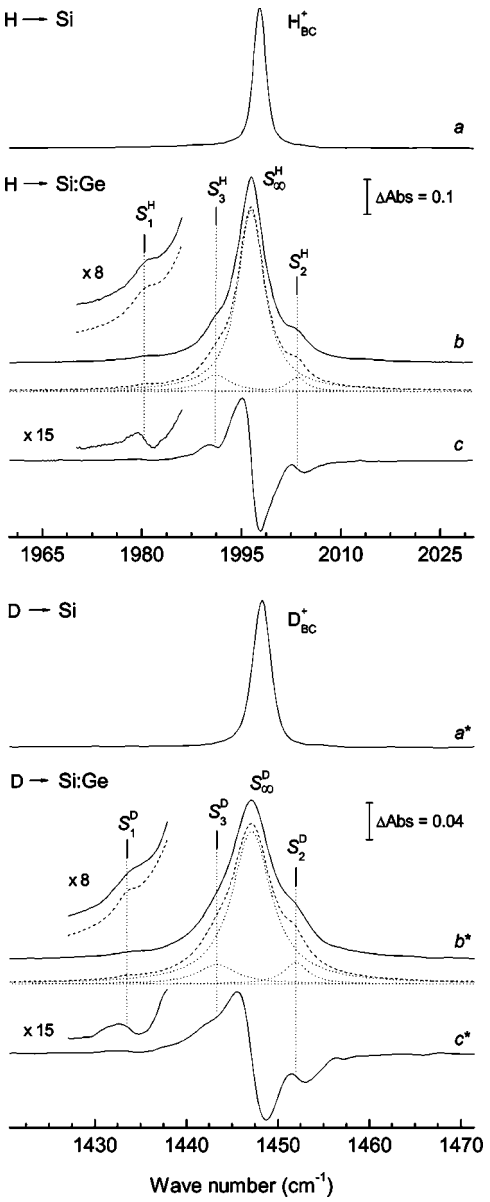

FIG. 2. Absorbance spectra observed in pure Si implanted with protons (curve *a*) and deuterons (curve a^*) compared with those recorded on Si:Ge implanted with protons (curve *b*) and deuterons (curve b^*), respectively. Curves *c* and c^* depict the first derivatives of spectra *b* and $b*$, where the components S_∞, S_1, S_2 and S_3 are more clearly resolved.

The absorbance spectra were calculated with background spectra recorded under the same conditions on the same samples before the implantations. The heat treatments of the samples were carried out by means of a resistive heater attached to the sample holder and connected to a temperature controller that allowed temperature stabilization within ±0.5 K at 8 K.

III. EXPERIMENTAL DATA

A. H_{BC}^{+} in Si:Ge

In Fig. 2, sections of the absorbance spectra measured at

TABLE I. Local mode frequencies (cm^{-1}) of hydrogen and deuterium observed in Si:Ge and Ge:Si compared with those estimated by *ab-initio* theory for the complexes shown in Fig. 1(b). The $Si:H^{+}_{BC}$ and $Ge:H^{+}_{BC}$ modes correspond to H^{+}_{BC} in pure Si and pure Ge, respectively. The configuration shifts, denoted as $\Delta\omega$, are given with respect to the frequency of S_{∞} in Si:Ge and G_{∞} in Ge:Si.

		Experimental		*Ab-initio*[a]	
Line	Site	ω	$\Delta\omega$	ω	$\Delta\omega$
$Si:H^{+}_{BC}$		1997.7	1.2		
		1448.4	1.3		
S^{H}_{∞}	$(Ge_sH^{+}_{BC})_{\infty}$	1996.5	…	2109	…
S^{D}_{∞}		1447.1	…	1501	…
S^{H}_{1}	$(Ge_sH^{+}_{BC})_{1}$	1980.4	−16.1	2091	−18
S^{D}_{1}		1433.5	−13.6	1485	−16
S^{H}_{2}	$(Ge_sH^{+}_{BC})_{2}$	2003.5	7.0	2123	14
S^{D}_{2}		1452.0	4.8	1510	9
	$(Ge_sH^{+}_{BC})_{3b}$			2119	10
				1508	7
S^{H}_{3}	$(Ge_sH^{+}_{BC})_{3a}$	1991.2	−5.3	2108	−1
S^{D}_{3}		1443.4	−3.8	1500	−1
$Ge:H^{+}_{BC}$		1793.9	−2.2		
		1293.1	−1.6		
G^{H}_{∞}	$(Si_sH^{+}_{BC})_{\infty}$	1796.1	…	1897	…
G^{D}_{∞}		1294.7	…	1345	…
G^{H}_{1}	$(Si_sH^{+}_{BC})_{1}$	1832.8	36.6	1936	39
G^{D}_{1}		1326.5	31.8	1376	31
G^{H}_{2}	$(Si_sH^{+}_{BC})_{2}$	1787.9	−8.2	1887	−10
G^{D}_{2}		1289.2	−5.3	1338	−7
	$(Si_sH^{+}_{BC})_{3b}$			1892	−5
				1341	−4
G^{H}_{3}	$(Si_sH^{+}_{BC})_{3a}$	1800.0	3.9	1899	2
G^{D}_{3}		1297.5	2.8	1346	1

[a]from Ref. 17.

~8 K after low temperature proton and deuteron implantation into pure silicon are shown, respectively, in curves *a* and *a**. Proton implantation is known to produce one strong line at 1998 cm^{-1} assigned to the A_{2u} LVM of H^{+}_{BC}. The similar LVM of D^{+}_{BC} is observed at 1448 cm^{-1} (curve *a**). The absorbance spectra recorded when similar experiments are performed with Si:Ge are shown for the same spectral range in curves *b* and *b** of Fig. 2. Proton implantation into Si:Ge gives rise to an intense line at 1996 cm^{-1}, labeled S^{H}_{∞}, together with three weaker lines at 1980, 2004 and 1991 cm^{-1}. Anticipating our assignments below, the latter lines are denoted S^{H}_{1}, S^{H}_{2} and S^{H}_{3}, respectively. A similar set of lines is observed when the experiments are repeated with deuterons, but the frequencies are all shifted downwards by a factor close to $\sqrt{2}$ (see curve *b**). This establishes that the lines represent local vibrational modes of hydrogen bonded to heavier elements, which almost certainly are silicon or germanium. The spectra displayed in curves *b* and *b** have been fitted with a sum of four Lorentzians, and the resulting best fit is also shown in the figure together with the individual components. The line positions obtained from the fits are compiled in Table I. Since no long-range diffusion of hydrogen is expected and since similar experiments in pure Si and pure Ge result in hydrogen in a fundamental configuration, i.e. occupying an antibonding site or a bond center site, we expect the same to happen in Si:Ge. However, hydrogen in the antibonding site is expected to have a lower frequency than those observed here, as it is the case of the antibonding hydrogen in the H^{*}_{2} defect in Si that vibrates at 1838 cm^{-1}.[39] On the other hand, the H mode frequencies observed in Si:Ge are very similar to that of H^{+}_{BC} in pure Si (see Table I). Thus, the S^{H}_{∞} line should correspond to quasi-isolated H^{+}_{BC} in Si:Ge. Moreover, the lines S^{H}_{1}, S^{H}_{2}, and S^{H}_{3} are probably related to H^{+}_{BC} centers perturbed by nearby substitutional Ge atoms, since they are unobserved in pure Si and since the Ge concentration in Si:Ge by far exceeds the concentration of other impurity atoms and of defects created by the implantation process.

To confirm that the lines detected in Si:Ge are indeed all related to H^{+}_{BC} species, an isochronal annealing study was performed. The implanted samples were heat treated for 20 min at a series of increasing annealing temperatures be-

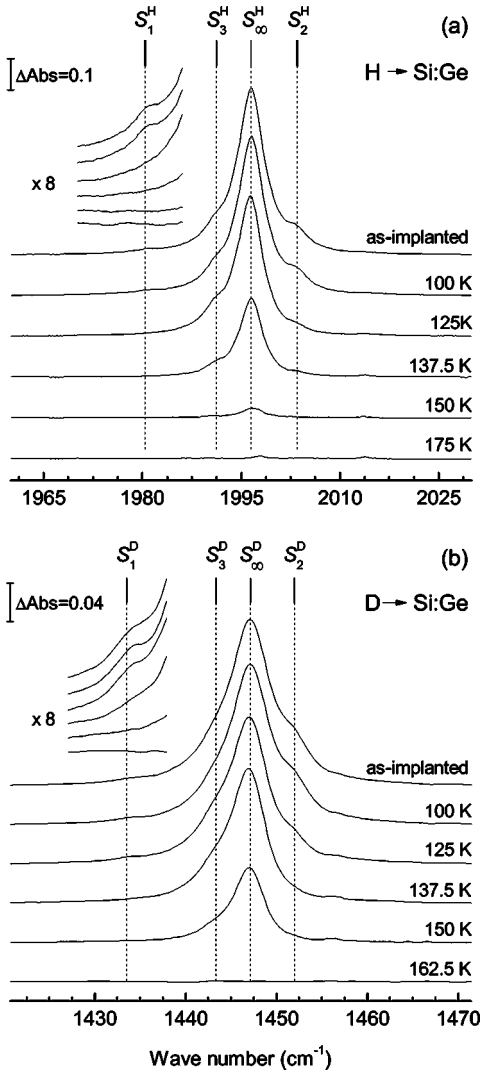

FIG. 3. Infrared absorbance spectra measured on the Si:Ge crystals implanted with protons (a) and deuterons (b) after 20 min heat treatment at the temperatures indicated in the figure. Magnified sections of the spectra are included to follow the annealing of the S_1 lines, so that the temperature ordering from top to bottom is the same as for the full spectra.

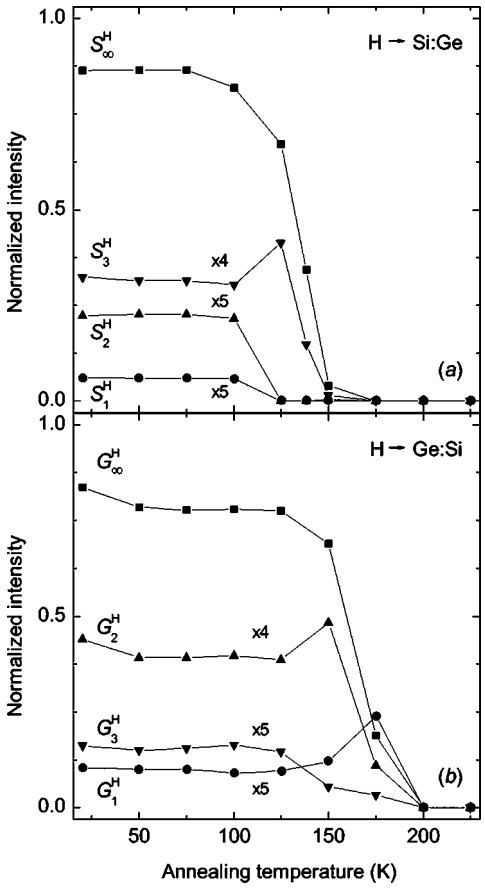

FIG. 4. Intensity of the LVM modes detected in proton-implanted (a) Si:Ge and (b) Ge:Si plotted versus the annealing temperature.

tween 50 K and room temperature. After each annealing the samples were cooled down to ~8 K and the infrared absorption spectrum was recorded. Infrared absorption spectra measured during the annealing sequence are depicted in Fig 3. These spectra have also been fitted with a sum of four Lorentzian profiles with center positions fixed to the values obtained from fitting the spectra measured just after the implantation. The intensities of the S_∞^H, S_1^H, S_2^H, and S_3^H lines are displayed against annealing temperature in Fig. 4(a). Although the lines display slightly different annealing behaviors, they all anneal out at approximately the same temperatures (125–150 K). No other absorption lines detected in the spectra have a similar annealing dependence. In the deuteron-implanted sample the corresponding deuterium modes display a similar annealing behavior but shifted to slightly higher temperature, which shows that the hydrogen atom plays an active role in the annealing. The annealing behavior displayed by the hydrogen-related lines in Si:Ge is similar to that reported for H_{BC}^+ in pure Si and also observed here for the H_{BC}^+ line in pure Si. On this basis, it is concluded that the lines are related to stretching modes of different configurations of H_{BC}^+ in Si:Ge.

B. H_{BC}^+ in Ge:Si

The absorbance spectra recorded on pure Ge and on Ge:Si after proton or deuteron implantation are shown in Fig. 5. All spectra have been measured at 8 K without any intervening heating of the crystals after the low temperature implantations. The spectrum of the proton-implanted Ge:Si sample (curve *b*) reveals a series of lines in the typical range of the Ge—H stretch modes. We denote the intense line at 1796 cm^{-1} by G_∞^H and the three less prominent lines at 1833, 1788, and 1800 cm^{-1} we label G_1^H, G_2^H, and G_3^H, as can be seen in the figure. The observed lines shift down in frequency by a factor close to $\sqrt{2}$ when deuterons are implanted (curve b^*) instead of protons. Hence, the lines represent local vibrational modes of hydrogen bond to heavier elements, which almost certainly are Ge and/or Si. The G_3^D line is weak and masked by the intense G_∞^D line in the spectrum. However, this line could be revealed as a change of the gradient

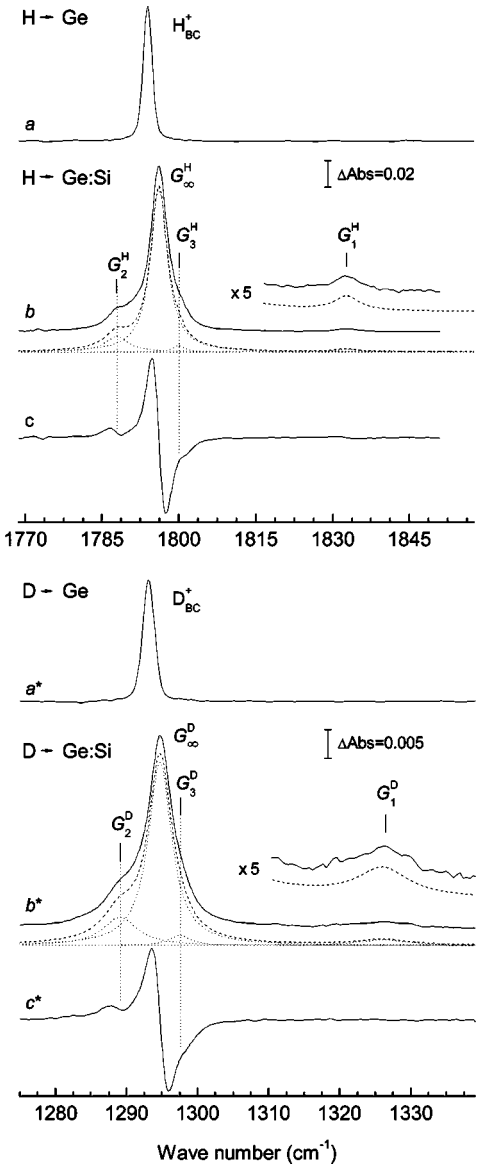

FIG. 5. Sections of infrared absorbance spectra recorded on pure Ge implanted with protons (curve *a*) or deuterons (curve a^*) compared with spectra recorded on Ge:Si after similar implantations (curves *b* and b^*). The weak G_3 line is more clearly resolved in the plots of the first derivatives of the spectra (curves *c* and c^*).

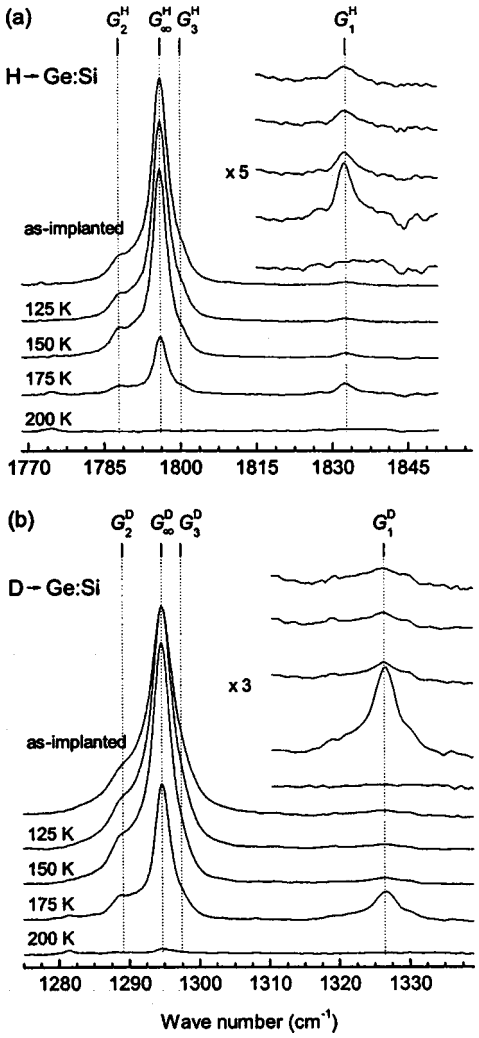

FIG. 6. Infrared absorbance spectra recorded on (a) proton- and (b) deuteron-implanted Ge:Si subjected to a series of 20 min anneals. The magnified sections of the spectra are plotted in the same order of temperatures as the corresponding full spectra.

in the first-derivative spectrum that is shown in curve c^*. The absorbance spectra observed after implantation of hydrogen and deuterium into pure Ge are also shown in curves *a* and a^*, respectively. In pure Ge implanted with protons (deuterons) a single line is detected at 1794 cm^{-1} (1293 cm^{-1}), which was previously assigned to H^+_{BC} (D^+_{BC}). The remarkable similarity between the spectra recorded on proton-implanted Ge:Si and pure Ge suggests that the G^H_∞ line is related to *isolated* H^+_{BC} defects. Furthermore, the G^H_1, G^H_2, and G^H_3 modes most likely originate from hydrogen located at bond center sites with a Si atom in a nearby substitutional site, owing to the fact that they are detected only in the Si-doped material. The annealing behavior of the modes supports this assignment. Infrared absorbance spectra of the implanted Ge:Si were recorded at 8 K after each 20 min anneal at temperatures between 50 K and room temperature. The spectra obtained are shown in Fig. 6. The intensities of the individual lines were determined from fitting to the spectra a sum of four Lorentzians. The positions of the Lorentzians were fixed at the values obtained from the best fit to the spectra recorded immediately after the implantation. The intensities of the individual components are plotted versus annealing temperature in the bottom half of Fig. 4. Although the detailed annealing behavior of the modes differ, they all have a fairly constant intensity up to ~125 K and anneal out at about 200 K. This behavior is essentially the same as that previously reported for H^+_{BC} in pure Ge and observed here for the H^+_{BC} line in the pure Ge sample implanted with protons. Such an observation provides strong support for the assignment of the lines in Ge:Si to different configurations of H^+_{BC} defects, which was given above.

TABLE II. The square of the H_{BC}^{+} stretching mode frequencies obtained for the three nearest neighbor configurations. μ_H, μ_D, μ_s, and μ_g are the inverse masses of H, D, Si, and Ge, respectively. f_s is the force constant of Si—H and f_g is the force constant for a Ge—H bond. The deuterium mode frequencies (ω_D) have the same dependence but with μ_H replaced by μ_D. The third column shows the square of the ratios between the hydrogen and deuterium frequencies. The ratio between the f_s and f_g force constants is denoted $\lambda = f_s/f_g$. It should be noted that f_s and f_g may differ for Si—H—Si, Si—H—Ge, and Ge—H—Ge.

Mode config.	ω_H^2	$\gamma^2 = \omega_H^2/\omega_D^2$
Si—H—Si	$\omega_{H,Si}^2 = f_s(2\mu_H + \mu_s)$	$\gamma_{Si}^2 = \dfrac{2\mu_H + \mu_s}{2\mu_D + \mu_s}$
Si—H—Ge	$\omega_{H,SiGe}^2 = 1/2\{f_g(\mu_g + \mu_H) + f_s(\mu_s + \mu_H) + \sqrt{4f_g f_s \mu_H^2 + [f_g(\mu_g + \mu_H) - f_s(\mu_s + \mu_H)]^2}\}$	$\gamma_{SiGe}^2 = \dfrac{(\mu_g + \mu_H) + \lambda(\mu_s + \mu_H) + \sqrt{4\lambda\mu_H^2 + [(\mu_g + \mu_H) - \lambda(\mu_s + \mu_H)]^2}}{(\mu_g + \mu_D) + \lambda(\mu_s + \mu_D) + \sqrt{4\lambda\mu_D^2 + [(\mu_g + \mu_D) - \lambda(\mu_s + \mu_D)]^2}}$
Ge—H—Ge	$\omega_{H,Ge}^2 = f_g(2\mu_H + \mu_g)$	$\gamma_{Ge}^2 = 2\mu_H + \mu_g / 2\mu_D + \mu_g$

IV. ANALYSIS AND DISCUSSION

A. H_{BC}^{+} simple vibrational model

The experimental data strongly suggest that the infrared lines detected in the proton-implanted Si:Ge and Ge:Si originate from stretching modes of some sort of H_{BC}^{+}. There are three possible nearest-neighbor configurations for this defect in SiGe, where hydrogen is located between and bonded to (i) two Si atoms (Si—H—Si), (ii) one Si and one Ge (Si—H—Ge) and (iii) two Ge atoms (Ge—H—Ge). First, we discuss the expected vibrational properties of these configurations in order to guide the identification of the nearest neighbor arrangements associated with each of the observed modes.

It has been demonstrated that a very good description of the hydrogen vibrational mode of H_{BC}^{+} may be obtained with a vibrational model of the triatomic molecule shown in Fig. 1(a), which includes H (or D) and its two adjacent atoms X_i-H ($i=1,2$).[40] These findings indicate that the frequency of the hydrogen mode primarily depends on the masses of the H isotope and the two X_i-H atoms, and the potential energy associated with stretching of the two X_i-H bonds. If we assume a harmonic potential for each X_i-H bond, the hydrogen (deuterium) mode frequencies ω_H (ω_D) can be calculated with standard techniques[41] and the results for each nearest-neighbor configuration are summarized in Table II. The squares of the corresponding ratios between the hydrogen and deuterium frequencies (ω_H/ω_D), which we label γ_{Si}, γ_{SiGe}, and γ_{Ge}, are also given in the table. We note from the table that within the harmonic approximation the ratios γ_{Si} and γ_{Ge} of Si—H—Si and Ge—H—Ge, respectively, are independent of the force constants f_s and f_g. Although the force constant for a Si—H—Si unit (or a Ge—H—Ge unit) may differ from one H_{BC}^{+} site to another, due to differences in the configuration of the next neighboring atoms, the ratio γ_{Si} (or γ_{Ge}) is expected to be the same for all Si—H—Si (or Ge—H—Ge) bond center sites. Moreover, γ_{SiGe} depends only on the ratio $\lambda = f_s/f_g$. Consequently, γ_{SiGe} should be almost equal for different Si—H—Ge units provided that λ is similar for all Si—H—Ge defects. In Fig. 7(a), ratios $\gamma = \omega_H/\omega_D$ are depicted for the three nearest neighbor configurations as a function of λ. As can be seen from the figure, for values of λ in the interval 1.0–1.7, the value of the ratio γ_{SiGe} is expected to lie between the values of γ_{Ge} and γ_{Si}.

B. Isotopic shift analysis: nearest neighbor configurations

The experimental ratios γ_{Si}, γ_{SiGe}, and γ_{Ge} are depicted in Fig. 7(b) for the hydrogen modes in Si:Ge and Ge:Si, together with the ratios for H_{BC}^{+} in pure Si and pure Ge. The experimental ratios are slightly lower than those calculated with our model. This discrepancy is primarily due to anharmonicity. In the Appendix we describe how anharmonicity affects the isotope shifts of H_{BC}^{+}. At this point, we simply summarize the results and shall refer to the appendix for further details. Anharmonicity lowers the harmonic ratios γ_{Si}, γ_{SiGe}, and γ_{Ge} and to a good approximation we may apply a common factor $\alpha = 0.9845$ to write

$$\gamma_k^{\text{anharm}} = \alpha\gamma_k \quad \text{with } k = \text{Si, SiGe, Ge}. \tag{1}$$

As the correction factor is the same for all nearest-neighbor configurations, it leaves the behavior indicated in Fig. 7(a) qualitatively unchanged.

The calculated harmonic ratios γ_{Si}, γ_{SiGe}, and γ_{Ge} have been scaled by the factor $\alpha = 0.9845$ and plotted in Fig. 7(b) together with the experimental values. The experimental values of ω_H/ω_D are clearly separated into three groups. On the basis of the above discussion, the fact that the S_∞, S_2, and S_3 lines display virtually the same value as Si:H_{BC}^{+} provides strong evidence for the assignment of these lines to H_{BC}^{+} with the Si—H—Si nearest-neighbor configuration. A similar argument establishes that the G_∞, G_2, and G_3 lines arise from H_{BC}^{+} centers with the configuration Ge—H—Ge.

The S_1 and G_1 lines display a very similar value of the ratio ω_H/ω_D, which, however, is distinguishable from those

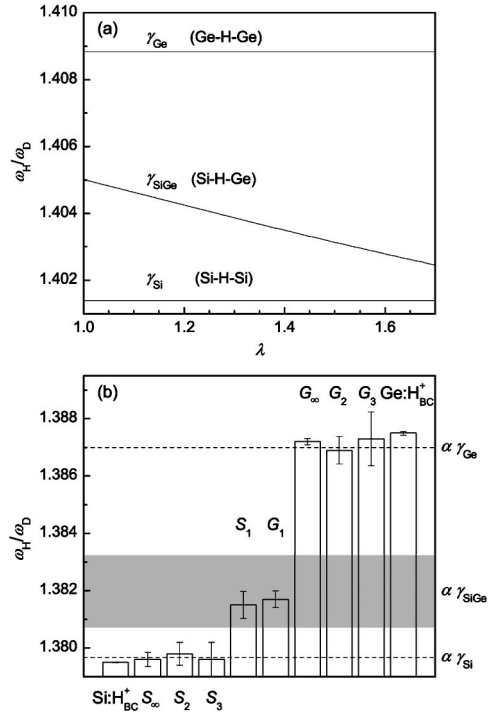

FIG. 7. (a) Calculated dependence of the isotopic shifts of Si—H—Si, Si—H—Ge, and Ge—H—Ge for values of $\lambda = f_s/f_g$ in the range 1.0–1.7. This dependence has been calculated with expressions given in Table II. (b) Experimental isotopic shifts of the LVMs detected in Si:Ge and Ge:Si, together with the calculated isotopic shifts shown in the upper half of the figure but scaled by the factor $\alpha = 0.9845$. The shaded area represents the interval of scaled γ_{SiGe} values that corresponds to values of λ in the range 1.0–1.7. The experimental ratios ω_H/ω_D observed for H^+_{BC} in pure Si and pure Ge are included and labeled by Si:H^+_{BC} and Ge:H^+_{BC}, respectively.

of Si:H^+_{BC} and Ge:H^+_{BC}. This strongly suggests that the S_1 and G_1 lines arise from two H^+_{BC} centers with a common nearest-neighbor configuration and different from Si—H—Si and Ge—H—Ge. This indicates that the nearest-neighbor configuration is Si—H—Ge. Moreover, the calculated (and scaled) values of γ_{SiGe} are in agreement with the observed values, as can be seen from Fig. 7(b). From Fig. 7, the experimental ratios ω_H/ω_D for the S_1 and G_1 lines correspond to a value of λ of 1.4, which agrees with the value $\lambda = 1.2$ that is calculated from the f_s and f_g force constant values estimated in the Appendix. On this basis, we ascribe the S_1 and G_1 modes to interstitial hydrogen in the Si—H—Ge configuration.

C. Second- and third-nearest neighbor configurations

The above analysis shows that the S_∞, S_2, and S_3 lines originate from three different H^+_{BC} centers with H located between two silicon atoms (Si—H—Si), whereas the G_∞, G_2, and G_3 modes correspond to H^+_{BC} centers with the Ge—H—Ge nearest-neighbor configuration. Moreover, the S_1 and G_1 arise from H^+_{BC} centers where H bonds to one Si and one Ge (Si—H—Ge). Now, we discuss the most likely next-neighbor configurations associated with the observed modes.

Substitutional Ge in silicon leads to four Si—Ge bonds that are longer than the averaged Si—Si bond. As a result, substitutional Ge induces a strain field around its site that causes either compression or elongation of the surrounding Si—Si bonds. Similarly, substitutional Si in germanium leads to four Si—Ge that are shorter than the averaged Ge—Ge bond length, which also induces the compression or elongation of the surrounding Ge—Ge bonds. These effects have consequences on the stretching frequency of H^+_{BC} when hydrogen is located at bond center sites. As mentioned in the Introduction, the H^+_{BC} structure is the result of two opposed energy terms: (a) the energy gain associated with the formation of the three-atom bond (X_1-H-X_2) and (b) the energy rise associated with the outwards displacement of the two host atoms neighboring the H atom. It is energetically more favorable to add a hydrogen atom to an elongated site, because less energy is required to move the the two neighboring host atoms outwards. In such a situation, the resulting X_i-H bond length will be slightly larger than for an unstrained bond center site. Contrarily, a compressed bond center site will lead to shorter X_i-H bonds because more energy is needed to relax the host atoms. It is well known in molecular spectroscopy that the stretch frequency of a bond decreases when the bond length increases. Therefore, the H^+_{BC} stretch frequency at strained sites will differ from that of isolated H^+_{BC}, i.e., lower frequencies for elongated sites and higher frequencies for compressed sites. In Si:Ge, the local strain is induced by substitutional Ge atoms, whereas in Ge:Si the strain is produced by substitutional Si atoms, due to the fact that these are by far the most abundant impurity atoms in each sample. In this context, it is plausible that the S_∞, S_2, and S_3 mode frequencies result from different local strains induced by different arrangements of Si and Ge in the vicinity of the Si—H—Si unit. Likewise, the G_∞, G_2, and G_3 modes correspond to different arrangements of Si and Ge in the vicinity of the Ge—H—Ge unit.[42]

The strain induced by the minority species is expected to become more pronounced for bond center sites closer to the perturbing atom. Taking into account the low concentration of the minority species in the samples, it is most probable that these are distant from the bond center site. Thus, we ascribe the most intense lines of the spectra, i.e., S_∞ in Si:Ge and G_∞ in Ge:Si, to H^+_{BC} defects where the minority species are located remotely enough from the H^+_{BC} so that they do not cause a resolvable change of its stretching frequency. These quasi-isolated centers are labeled in the present paper as $(Ge_sH^+_{BC})_\infty$ for Si:Ge and $(Si_sH^+_{BC})_\infty$ for Ge:Si. We shall return to this point in the next subsection. The small difference between the S_∞ and G_∞ mode frequencies and those of Si:H^+_{BC} and Ge:H^+_{BC} is due to the different averaged Si—Si and Ge—Ge bond lengths in the Si:Ge and Ge:Si samples when compared to the bond lengths in pure Si and pure Ge, respectively. In the Si:Ge crystals the regular Si—Si bond length is expected to be somewhat larger than in elemental Si.[30] This produces the downward shift of the S_∞ line, whereas in Ge:Si the averaged Ge—Ge bond lengths are slightly smaller,[30] yielding an enhancement of the G_∞ mode frequency.

TABLE III. Normalized experimental intensities I_{exp} of hydrogen modes of Si:Ge and Ge:Si compared with the abundance p of the centers to which they are ascribed. The latter values are calculated assuming a random distribution of H_{BC}^{+} in Si:Ge and Ge:Si crystals with randomly distributed Si and Ge.

Sample	Line	Site	I_{exp}	p
Si:Ge	S_{∞}^{H}	$(Ge_sH_{BC}^{+})_{\infty}$	0.86(2)	0.834(2)
	S_1^{H}	$(Ge_sH_{BC}^{+})_1$	0.012(8)	0.015(2)
	S_2^{H}	$(Ge_sH_{BC}^{+})_2$	0.05(1)	0.045(2)
	S_3^{H}	$(Ge_sH_{BC}^{+})_{3a}$	0.08(1)	0.091(2)
Ge:Si	G_{∞}^{H}	$(Si_sH_{BC}^{+})_{\infty}$	0.84(3)	0.785(2)
	G_1^{H}	$(Si_sH_{BC}^{+})_1$	0.02(1)	0.019(2)
	G_2^{H}	$(Si_sH_{BC}^{+})_2$	0.11(2)	0.057(2)
	G_3^{H}	$(Si_sH_{BC}^{+})_{3a}$	0.03(2)	0.114(2)

The S_2 and S_3 mode frequencies indicate that they correspond to Si—H_{BC}^{+}—Si sites that are compressed and elongated, respectively, due to nearby Ge atoms. These defects probably involve only one Ge atom because the concentration of Ge in our crystals is low and germanium is immobile under our experimental conditions. Analogously, the G_2 and G_3 lines should correspond to Ge—H_{BC}^{+}—Ge perturbed by a single nearby silicon atom. As mentioned above, substitutional Ge in silicon forms four Si—Ge bonds which are longer than the natural Si—Si bonds in silicon. In Si:Ge, the nature of the local strain on the H_{BC}^{+} depends on the orientation of the Si—H—Si unit with respect to the Si—Ge bonds. It is conventional wisdom that the longer Si—Ge bonds lead to the compression of the adjacent Si—Si bonds, while Si—Si bonds with a bond center position within in the plane perpendicular to the Si—Ge bond are expanded. Therefore, the Ge atom induces an excess compression, when compared with quasi-isolated H_{BC}^{+}, for the $(Ge_sH_{BC}^{+})_2$ and $(Ge_sH_{BC}^{+})_{3b}$ sites, shown in Fig. 1(b). Contrarily, H_{BC}^{+} should experience a tensile strain if Ge is placed in the 3a position. Thus, we ascribe the S_2 line to $(Ge_sH_{BC}^{+})_2$ or $(Ge_sH_{BC}^{+})_{3b}$ complexes, and the S_3 line to a weakly bound hydrogen-germanium complex in the $(Ge_sH_{BC}^{+})_{3a}$ configuration. In Ge:Si, the tensile character of Si—Ge bonds yields an inverse situation. Namely, the $(Si_sH_{BC}^{+})_2$ and $(Si_sH_{BC}^{+})_{3b}$ sites should be elongated and the $(Si_sH_{BC}^{+})_{3a}$ site is compressed due to the nearby Si atom. Hence, we associate the $(Si_sH_{BC}^{+})_2$ or $(Si_sH_{BC}^{+})_{3b}$ sites with the lower frequency line G_2 and ascribe the G_3 line to $(Si_sH_{BC}^{+})_{3a}$ complexes. It is difficult, however, to distinguish which of the two configurations gives rise to the S_2 (or G_2) band. Nevertheless, the magnitude of the line shifts with respect to the central line S_{∞} (or G_{∞}), denoted here as $\Delta\omega$ may give some further insight on this issue. The configuration shifts $\Delta\omega$ are reproduced in Table I. As can be seen in the table, the shifts of the S_2 and G_2 lines are larger than the magnitude of the shifts measured for the S_3 and G_3 lines, respectively. This may indicate that the hydrogen-germanium and hydrogen-silicon distance is smallest in the complexes responsible for the S_2 and G_2 lines, respectively. Therefore, we favor the assignment of the S_2 and G_2 lines, respectively, to $(Ge_sH_{BC}^{+})_2$ and $(Si_sH_{BC}^{+})_2$. In Si:Ge, the effect from a substitutional Ge in the 3b site on the H_{BC}^{+} frequency is probably small so that the mode of the $(Ge_sH_{BC}^{+})_{3b}$ configuration is hidden below the S_0. Likewise, the $(Si_sH_{BC}^{+})_{3b}$ mode in Ge:Si should be undiscerned from the G_0 line. However, we cannot rule out completely that the S_2 and G_2 lines arise from $(Ge_sH_{BC}^{+})_{3b}$ and $(Si_sH_{BC}^{+})_{3b}$ sites, respectively, in Si:Ge and Ge:Si.

D. Mode intensities

Now we investigate whether the intensities of the lines are consistent with the above assignments. Since the effective charge is expected to be about the same for the different H_{BC}^{+} modes their normalized intensities should be similar to their abundances, if we assume a random distribution of Si and Ge and that all H_{BC}^{+} configurations have the same formation probability during low temperature proton implantation. Table III compares the calculated probabilities of $(Ge_sH_{BC}^{+})_j$ and $(Si_sH_{BC}^{+})_j$ sites with the experimental normalized intensities of the corresponding infrared lines. The statistical calculation has been carried out on a shell of 20 atoms around the hydrogen. As can be seen in the table, the experimental intensities are close to the random distributions, giving further support for our assignments. However, there is a deviation between the intensives and the random probabilities for the G_2 and G_3 modes. We believe that this reflects a real tendency of hydrogen to become trapped at elongated sites in Ge:Si, like $(Si_sH_{BC}^{+})_2$, presumably because the energy required for the outwards relaxation of the two Ge atoms to accommodate H is lower, unlike $(Si_sH_{BC}^{+})_{3a}$ sites where the required energy is higher.

As described in the Introduction, a Laplace-DLTS investigation of Si doped with Ge to concentrations similar to that of our Si:Ge crystals yielded the identification of a new donor level named $E3'$(Ge), and ascribed to the $H_{BC}(0/+)$ transition occurring in a complex with the $(Ge_sH_{BC}^{+})_2$ structure.[35] The authors reported an overpopulation for $(Ge_sH_{BC}^{+})_2$ species as compared to a random distribution. This effect was explained as the result of an ultrafast migration of the implants during the final stage of thermalization, in conjunction with the lowering of the barrier for capture of hydrogen at bond center sites close to Ge, as compared to the barrier for hydrogen capture at unperturbed bond center sites.

Such an overpopulation of $(Ge_sH^+_{BC})_2$ sites has not been observed in the experiments presented here. We note, however, that there are significant differences in the experimental conditions of the two studies: (a) the H-implantation doses are more than 10^4 times higher in our experiments, and (b) the implantation temperature is below 20 K in the present work and about 60 K for the DLTS investigations. The low temperature and the relatively high implantation dose in our experiments result in an nonequilibrium situation where the Fermi level is undefined after the implantation, whereas in the DLTS experiments this level is determined by the *n*-type doping of the crystal. In a single experiment, where we used a lower implantation dose, we observed an overpopulation of $(Ge_sH^+_{BC})_2$ sites. This suggests that the damage reduces the differences between the barriers for hydrogen capture in distinct H^+_{BC} sites.

E. Isochronal annealing

Although the annealing behaviors of the lines are roughly similar, there are slight differences. The results of the isochronal annealing series are depicted in Fig. 4. Let us start by comparing the annealing response of the centers with configuration Si—H—Ge with that of the quasi-isolated H^+_{BC}. As can be seen in the figure, the $(Ge_sH^+_{BC})_1$ center in Si:Ge is found to be less thermally stable than $(Ge_sH^+_{BC})_\infty$, whereas in Ge:Si, the $(Si_sH^+_{BC})_1$ complexes are formed transiently when $(Ge_sH^+_{BC})_\infty$ anneals. A simple explanation is that Ge—H bonds are weaker than Si—H bonds and, thus, the Si—H—Ge configuration is expected to be less stable than Si—H—Si but more stable than Ge—H—Ge defects.

Our annealing data show that when the S_2 and G_3 modes anneal there is an increase in the S_3 and G_2 lines intensities, respectively. This is fully consistent with the expectation that compressed H^+_{BC} sites, like $(Ge_sH^+_{BC})_2$ and $(Si_sH^+_{BC})_{3a}$, should be less stable than elongated bond center sites, since the compression opposes the outwards relaxation required to accommodate the hydrogen. Contrarily, elongated configurations should be more stable, because less energy is needed to move the two neighboring Si atoms. Under this picture one would expect the quasi-isolated H^+_{BC}, $(Ge_sH^+_{BC})_\infty$ in Si:Ge, to anneal out at an intermediate temperature with respect to those of the $(Ge_sH^+_{BC})_2$ and $(Ge_sH^+_{BC})_{3a}$ sites. Analogously, the G_0 mode in Ge:Si would anneal out at a temperature between those of the $(Si_sH^+_{BC})_{3a}$ and $(Si_sH^+_{BC})_2$ sites. However, the intensities of the S_0 and G_0 modes seem to reach half of their maximum intensities at about the same temperatures as the $(Ge_sH^+_{BC})_{3a}$ and $(Si_sH^+_{BC})_2$ elongated sites, respectively. A simple explanation is that entropy favors sites with higher abundances over the others. Nevertheless, we indeed observe a decrease of the S_0 and G_0 modes' intensities at the same temperatures where the intensities of the S_3 and G_2 modes increases. These observations lend further support to the assignments made in Sec IV C.

F. Comparison with *ab-initio* calculations

A further confirmation of our assignments is provided by LVM frequencies calculated using *ab-initio* density-functional theory. As mentioned in the Introduction, the results of an investigation based on cluster theory applied to a 64-atom supercell and that considered different forms of H^+_{BC} in Si with 1.6% Ge and Ge with 1.6% Si have been published recently.[17] The complexes investigated in that work are indicated in Fig. 1(b) and the corresponding H and D mode frequencies are compared with our experimental data in Table I. The authors reported overestimated frequencies due the fact that anharmonicity has not been accounted for in the calculations. However, the frequency shifts $\Delta\omega$ should be almost unaffected by anharmonicity, because the mode frequencies are largely determined by the harmonic part of the potential energy. The values of $\Delta\omega$ obtained from the *ab-initio* frequencies are also given in Table I. As can be seen from the table, the frequency of H^+_{BC} drops (rises) by about 18 cm^{-1} (39 cm^{-1}) when the Ge (Si) atom is moved from distant sites to the nearest-neighbor site. This behavior is in fair quantitative agreement with our observations for the S_1 and G_1 bands. In addition, the frequency of H^+_{BC} is found to increase when Ge is moved from unstrained sites to $(Ge_sH^+_{BC})_{3b}$ and rises further when it is placed in the second-nearest neighbor site $(Ge_sH^+_{BC})_2$. Moreover, the frequency found for $(Ge_sH^+_{BC})_{3a}$ is lower than that of $(Ge_sH^+_{BC})_\infty$. Furthermore, the magnitude of $\Delta\omega$ estimated for $(Ge_sH^+_{BC})_2$ is larger than that of $(Ge_sH^+_{BC})_{3b}$ sites, which gives support to our assignment of the S_2 line to $(Ge_sH^+_{BC})_2$ defects. In Ge:Si, the mode frequencies of the $(Si_sH^+_{BC})_2$, $(Si_sH^+_{BC})_{3a}$, and $(Si_sH^+_{BC})_{3b}$ defects exhibit an opposite ordering to that of their counterparts in Si:Ge (see Table I). These theoretical findings are fully in qualitative accordance with our assignments.

G. Comparison with other H^+_{BC}-related complexes

Previous studies of proton-implanted Czochralski-Si have identified local LVMs of two oxygen-hydrogen complexes labeled OH_I and OH_{II}.[33] Based on the analysis of the observed hydrogen and oxygen modes and the results of *ab-initio* calculations, the modes were assigned to H^+_{BC} centers with an interstitial oxygen (O_i) located in the vicinity. The frequencies of H^+_{BC} modes of the OH_I and OH_{II} complexes are at 1879 and 1830 cm^{-1}, respectively. This suggests that the oxygen atom in both centers induces a dilative strain on the bond center site that accommodates the hydrogen atom. In addition, infrared absorption studies in carbon-rich Si implanted with protons revealed a weakly bound carbon-hydrogen complex labeled $(C—H)_I$ in the literature.[31] The observed H mode at 1885 cm^{-1} was ascribed to the stretching of H^+_{BC} centers with a substitutional carbon (C_s) atom in either the second- or third-nearest-neighbor site. The shifts in frequency of the H^+_{BC} mode of OH_I, OH_{II} and $(C—H)_I$ from that of isolated H^+_{BC} are significantly larger than the shifts measured here for the $(Ge_sH^+_{BC})_j$ complexes. This indicates that in silicon H^+_{BC} is considerably less affected by the presence of a nearby substitutional Ge than by O_i or C_s. We may obtain a rough estimate of the magnitude of the bond length change of the Si—H—Si unit induced by neighboring impurities. The stretching frequency associated with a given

bond depends on the bond length. For diatomic molecules, Morse[43] proposed the following empirical relation between the stretching frequency ω and the bond length R,

$$\omega R^{\alpha} = \text{const}, \tag{2}$$

where $\alpha \sim 3$. If we assume that this also holds true for the Si—H bonds in H_{BC}^{+} centers, it implies that a frequency change $\Delta\omega/\omega_0$, with respect to the frequency ω_0 of isolated H_{BC}^{+}, corresponds to a bond length change,

$$\frac{\Delta R}{R_0} \sim -\frac{1}{3}\frac{\Delta\omega}{\omega_0}, \tag{3}$$

where R_0 is the bond length associated with unperturbed H_{BC}^{+} centers. Using this relation, we find that $\Delta R/R_0$ is -1.2×10^{-3} and 0.9×10^{-3} for $(Ge_sH_{BC}^{+})_2$ and $(Ge_sH_{BC}^{+})_{3a}$, respectively. These values are indeed smaller than the 19×10^{-3}, 20×10^{-3} and 28×10^{-3} obtained for the $(C—H)_I$, OH_I and OH_{II} complexes, respectively. Since the bond length of the Si—H—Si structure will correlate with the Si—Si bond length before the hydrogen occupies the bond center site, we conclude that the local deformation induced by Ge in the silicon lattice is quite small compared with that imposed by substitutional carbon and interstitial oxygen. Our estimates of the Si—H—Si relaxation assume that the defects form a linear structure in which the angle between the two Si—H bonds is 180 deg. This may not be the case, since the Si—H—Si unit may adopt a puckered structure, like, e.g., interstitial oxygen in Ge.[44] Nevertheless, this effect will not change the above qualitative conclusion.

The annealing behavior of OH_I shows that this defect anneals out at about 130 K, where the OH_{II} defect grows in. The OH_{II} defect anneals out at about 240 K. Presumably, the OH_I defect transforms into OH_{II} at $\sim$130 K, whereas the annealing at 240 K represents the thermal stability of an OH complex. The $(C—H)_I$ center is thermally stable up to $\sim$200 K. Hence, the OH_{II} and $(C—H)_I$ centers are significantly more thermally stable than the isolated H_{BC}^{+} in silicon, which anneals at about 150 K. In contrast, the $(Ge_sH_{BC}^{+})_2$ and $(Ge_sH_{BC}^{+})_{3a}$ defects exhibit about the same thermal stability as the quasi-isolated H_{BC}^{+}. Hence, the thermal stability of the $(Ge_sH_{BC}^{+})_2$ and $(Ge_sH_{BC}^{+})_{3a}$, OH_{II} and $(C—H)_I$ complexes correlate with the values of $\Delta R/R_0$ stated above. This provides further support to our view that elongated bond center sites for hydrogen are thermally more stable and lead to lower stretch mode frequencies. However, we emphasize that the various forms of H_{BC}^{+} have much lower thermal stability than defects where hydrogen has been trapped at vacancies or silicon interstitials which are stable above room temperature. Thus, in the case of the H_{BC}^{+} defects in Si:Ge (or Ge:Si), the perturbing Ge (or Si) does not seem to yield a strong stabilization of H_{BC}^{+}. This has been confirmed by the *ab initio* total energy calculations mentioned above.[17] In this work it was found that the different structures of H_{BC}^{+} in Si:Ge are energetically degenerate within the accuracy of the method.

V. SUMMARY

In conclusion, we have carried out *in-situ*-type infrared absorption measurements on silicon- and germanium-rich SiGe after proton implantation at temperatures below 20 K. The low temperature infrared absorbance spectra of Si:Ge and Ge:Si reveal a strong band at $\sim$2000 cm^{-1} and 1800 cm^{-1}, respectively. Each of these bands contains one dominant line and three less prominent lines. Similar sets of lines are observed in both samples when deuterons are implanted but the frequencies are shifted by a factor close to $\sqrt{2}$. This unambiguously establishes that the lines represent local vibrational modes of hydrogen. The comparison of the Si:Ge and Ge:Si spectra with those recorded on pure Si and pure Ge, together with the annealing behavior of the lines, allow us to conclude that the modes arise from different forms of positively charged interstitial hydrogen placed at a bond center site between two Si, two Ge, and one Si and one Ge atoms. An analysis of the frequency ratios ω_H/ω_D allows us to determine the nearest-neighbor configuration of each H_{BC}^{+} center. The dominant lines of the spectra, namely S_∞ and G_∞, arise from quasi-isolated H_{BC}^{+} bonded to two Si and two Ge atoms, respectively. Moreover, the S_1 and G_1 lines correspond to H_{BC}^{+} bonded to one Si and one Ge atom in Si:Ge and Ge:Si. The remaining lines originate from H_{BC}^{+} that are perturbed by the minority species located in the second- and third-nearest neighbor substitutional sites. The observed line intensities and the annealing behaviors are fully in agreement with these assignments. In addition, our results have been compared with previous experimental studies and the results of *ab-initio* theory calculations. The earlier results corroborate our assignments of the observed lines. Our data shows that in dilute SiGe alloys the minority element produces only a small local strain on the lattice, unlike the case of substitutional carbon[31] and interstitial oxygen[33] in silicon which seem to impose a significant lattice deformation locally. As a result, the minority species in Si:Ge and Ge:Si does not give a strong thermal stabilization of bond-centered hydrogen.

ACKNOWLEDGMENTS

We thank Pia Bomholt for preparing the samples for optical measurements and John Lundsgaard Hansen for the RBS measurements. K. Bonde Nielsen, J. Coutinho, and R. Jones are acknowledged for a number of valuable discussions. This work has been supported by the Danish National Research Foundation through Aarhus Center for Advanced Physics (ACAP) and in Poland by the Committee for Scientific Research, Grant No. 4T11B02123. R. N. Pereira thank the ECCN Network for financial support.

APPENDIX: CONTRIBUTION OF ANHARMONICITY TO ISOTOPIC SHIFTS

It has been shown previously that the stretch mode vibration of H_{BC}^{+} in Si is very well described by a simple model based on the Si—H—Si linear unit, with two Si—H oscillators described by anharmonic potentials.[40] With this model the hydrogen stretch mode frequency may be expressed as

$$\omega_H = \sqrt{f_s(2\mu_H + \mu_s)} + \omega_{\text{anharm}}, \tag{A1}$$

with the anharmonic frequency correction ω_{anharm} given by

TABLE IV. A comparison between the experimental frequencies (cm^{-1}) of H^+_{BC} and D^+_{BC} and those calculated with the anharmonic model of Eq. (A3). The fitting parameters f_s (eV $Å^{-2}$), f_g (eV $Å^{-2}$), and A ($\times 10^{-15}$ eV $Å^{-2}$ s) are also given in the table.

	Exp.	Calc.	f_s	f_g	A	α
Si	1997.7 1448.4	1997.7 1448.4	8.1029	…	−1.0827	0.984 19
Ge	1793.9 1293.1	1793.9 1293.1	…	6.5736	−0.9385	0.984 69

$$\omega_{\text{anharm}} = A(2\mu_H + \mu_s) + B\sqrt{\mu_s(2\mu_H + \mu_s)}, \qquad \text{(A2)}$$

where A and B depend solely on the parameters defining the harmonic, cubic, and quartic terms of the potential energy.[40] Thus, A and B do not depend on which Si and H isotopes are involved. The deuterium frequency can be calculated with the same expressions but with the inverse mass μ_H substituted by μ_D. For silicon, the anharmonic correction reduces the harmonic frequency only by 6%–7%, with the first term in Eq. (A2) contributing ~70% to the overall correction. Therefore, the hydrogen mode frequency may be approximated by

$$\omega_H \approx \sqrt{f_s(2\mu_H + \mu_s)} + A(2\mu_H + \mu_s). \qquad \text{(A3)}$$

This simplification of the model is very well justified in the present analysis because we are exclusively focused on the description of hydrogen isotopic shifts, that are predominantly determined by the first term of the anharmonic correction (A2). In contrast, the silicon isotopic shifts are dominated by the last term of Eq. (A2), as discussed in Ref. 40.

Using Eq. (A3) we can calculate the ratio $\gamma_{Si}^{\text{anharm}} = \omega_H/\omega_D$ in Si (Si—H—Si configuration) that takes into account anharmonicity,

$$\gamma_{Si}^{\text{anharm}} = \alpha_{Si}\sqrt{\frac{2\mu_H + \mu_s}{2\mu_D + \mu_s}}, \qquad \text{(A4)}$$

where the factor α_{Si} is given by

$$\alpha_{Si} = \frac{1 + \frac{A}{\sqrt{f_s}}\sqrt{2\mu_H + \mu_s}}{1 + \frac{A}{\sqrt{f_s}}\sqrt{2\mu_D + \mu_s}}. \qquad \text{(A5)}$$

As can be seen in Eq. (A5), the anharmonic correction of the isotopic shift depends only on the ratio $A/\sqrt{f_s}$. The parameters A and f_s may be estimated by comparing the H and D experimental frequencies with those calculated with Eq. (A3). The results are shown in Table IV, together with the values of f_g and A estimated for the same defect in Ge. The frequencies of H^+_{BC} in Ge are calculated with Eq. (A3) but with μ_g instead of μ_s. There is only a difference of 0.0005 between the values of α for H^+_{BC} in Si and Ge (see Table IV). This is more than one order of magnitude lower than the difference between the ratios ω_H/ω_D obtained experimentally for H^+_{BC} in pure Si and pure Ge. Thus the anharmonic correction α is close to 1.0 and nearly the same for the nearest-neighbor configurations Si—H—Si and Ge—H—Ge. This implies that the change observed for the ratio ω_H/ω_D when we go from Si to Ge is largely determined by the harmonic part of the potential energy. The fact that the same scaling factor α applies for the two extreme configurations Si—H—Si and Ge—H—Ge suggests that this factor is also appropriate for the intermediate configuration Si—H—Ge. Hence, we use the correction factor $\alpha = 0.9845$ for all nearest neighbor configurations of H^+_{BC} in Si:Ge and Ge:Si.

*Electronic address: pereira@phys.au.dk

[1] H. J. Stein, Phys. Rev. Lett. **43**, 1030 (1979).
[2] M. Budde, Ph.D. Thesis, University of Aarhus, Denmark, 1998.
[3] M. Budde, C. Parks Cheney, G. Lüpke, N. H. Tolk, and L. C. Feldman, Phys. Rev. B **63**, 195203 (2001).
[4] M. Budde, G. Lüpke, C. Parks Cheney, N. H. Tolk, and L. C. Feldman, Phys. Rev. Lett. **85**, 1452 (2000).
[5] M. Budde, B. Bech Nielsen, C. Parks Cheney, N. H. Tolk, and L. C. Feldman, Phys. Rev. Lett. **85**, 2965 (2000).
[6] B. Holm, K. Bonde Nielsen, and B. Bech Nielsen, Phys. Rev. Lett. **66**, 2360 (1991).
[7] K. Bonde Nielsen, B. Bech Nielsen, J. Hansen, E. Andersen, and J. U. Andersen, Phys. Rev. B **60**, 1716 (1999).
[8] L. Dobaczewski, K. Bonde Nielsen, N. Zangenberg, B. Bech Nielsen, A. R. Peaker, and V. P. Markevich, Phys. Rev. B **69**, 245207 (2004).
[9] Y. V. Gorelkinskii and N. N. Nevinnyi, Pis'ma Zh. Tekh. Fiz. **13**, 105 (1987) [Sov. Tech. Phys. Lett. **13**, 45 (1987)].
[10] B. Bech Nielsen, K. Bonde Nielsen, and J. R. Byberg, in *Defects in Semiconductors 17*, edited by H. Heinrich and W. Jantsch (Materials Science Forum, Trans Tech, Aedermannsdorf, Switzerland, 1994), pp. 143–147, p. 909.
[11] B. Bech Nielsen, Phys. Rev. B **37**, 6353 (1988).
[12] B. D. Patterson, Rev. Mod. Phys. **60**, 69 (1988).
[13] C. G. Van de Walle, Y. Bar-Yam, and S. T. Pantelides, Phys. Rev. Lett. **60**, 2761 (1988).
[14] K. J. Chang and D. J. Chadi, Phys. Rev. Lett. **62**, 937 (1989).
[15] R. Jones, Physica B **170**, 181 (1991).
[16] S. K. Estreicher, Mater. Sci. Eng. Rep. **14**, 319 (1995).
[17] A. Balsas, V. J. B. Torres, J. Coutinho, R. Jones, B. Hourahine, P. R. Briddon, and S. Öberg, J. Phys.: Condens. Matter (to be published).
[18] Y. V. Gorelkinskii and N. N. Nevinnyi, Mater. Sci. Eng., B **36**, 133 (1996).

[19] See, for example, C. G. Van de Walle, in *Hydrogen in Semiconductors II*, edited by N. H. Nickel (Academic, New York, 1999), Vol. 61, pp. 241–281.
[20] *GeSi Strained Layers and Their Applications*, edited by A. M. Stoneham and S. C. Jain (Institute of Physics, Bristol, UK, 1995).
[21] H. G. Grimmeiss, Semiconductors **33**, 939 (1999).
[22] G. Abstreiter, H. Brugger, T. Wolf, H. Jorke, and H. J. Herzog, Phys. Rev. Lett. **54**, 2441 (1985).
[23] C. A. King, J. L. Hoyt, C. M. Gronet, J. F. Gibbons, M. P. Scott, and J. Turner, IEEE Electron Device Lett. **10**, 2323 (1989).
[24] U. Konig and H. Dambkes, Solid-State Electron. **38**, 1595 (1995).
[25] T. P. Pearsall, Mater. Sci. Eng., B **9**, 225 (1991).
[26] T. P. Pearsall, J. Bevk, L. C. Feldman, J. M. Bonar, J. P. Mannaerts, and A. Ourmazd, Phys. Rev. Lett. **58**, 729 (1987).
[27] J. C. Bean, Proc. Inst. Electr. Eng. **80**, 571 (1992).
[28] J. Mi, P. Letourneau, M. Judelewicz, M. Gailhanou, M. Dutoit, C. Dubois, and J. C. Dupuy, Appl. Phys. Lett. **67**, 259 (1995).
[29] L. J. Regolini, S. Bodnar, J. C. Oberlin, F. Ferrieu, M. Gauneau, B. Lambert, and P. Boucaud, J. Vac. Sci. Technol. A **12**, 1015 (1994).
[30] J. C. Aubry, T. Tyliszczak, A. P. Hitchcock, J.-M. Baribeau, and T. E. Jackman, Phys. Rev. B **59**, 12 872 (1999), and references therein.
[31] L. Hoffmann, E. V. Lavrov, B. Bech Nielsen, B. Hourahine, R. Jones, S. Öberg, and P. R. Briddon, Phys. Rev. B **61**, 16 659 (2000).
[32] O. Andersen, A. R. Peaker, L. Dobaczewski, K. Bonde Nielsen, B. Hourahine, R. Jones, P. R. Briddon, and S. Öberg, Phys. Rev. B **66**, 235205 (2002).
[33] B. Bech Nielsen, K. Tanderup, M. Budde, K. Bonde Nielsen, J. L. Lindström, R. Jones, S. Öberg, B. Hourahine, and P. Briddon, Mater. Sci. Forum **258–263**, 391 (1997).
[34] K. Bonde Nielsen, L. Dobaczewski, S. Søgård, and B. Bech Nielsen, Phys. Rev. B **65**, 075205 (2002).
[35] K. Bonde Nielsen, L. Dobaczewski, A. R. Peaker, and N. V. Abrosimov, Phys. Rev. B **68**, 045204 (2003).
[36] K. Irmscher, H. Klose, and K. Maass, J. Phys. C **17**, 6317 (1984).
[37] R. N. Pereira, L. Dobaczewski, and B. Bech Nielsen, Physica B **340–342**, 803 (2003).
[38] B. Hourahine, R. Jones, S. Öberg, P. R. Briddon, and T. Frauenheim, J. Phys.: Condens. Matter **15**, S2803 (2003).
[39] M. Budde, B. Bech Nielsen, R. Jones, J. Goss, and S. Öberg, Phys. Rev. B **54**, 5485 (1996).
[40] R. N. Pereira, T. Ohya, K. M. Itoh, and B. Bech Nielsen, Physica B **340–342**, 697 (2003).
[41] E. B. Wilson, J. C. Decius, and P. C. Cross, *Molecular Vibrations: The Theory of Infrared and Raman Vibrational Spectra* (Dover, New York, 1980).
[42] Note that the mass of the system changes from one next neighbor configuration to another, depending on the number and location of atoms of the minority species in the vicinity. This mass change could influence the bondlengths and frequencies of the different defect configurations. However, the contribution to the oscillator effective mass from atoms farther away than the two nearest neighbors of hydrogen is virtually zero and the consequent change in bond length and frequency is negligible.
[43] P. M. Morse, Phys. Rev. **34**, 57 (1929).
[44] E. Artacho, F. Ynduráin, B. Pajot, R. Ramírez, C. P. Herrero, L. I. Khirunenko, K. M. Itoh, and E. E. Haller, Phys. Rev. B **56**, 3820 (1997).